A Wideband mmWave Antenna Element with an Unbalanced Feed

David W. Landgren, Kevin R. Cook, Daniel J.P. Dykes, Jonathan Perez, Phillip R. Bowden, and Kenneth W. Allen*

***Abstract*—In this article an ultra-wideband (UWB), millimeter wave (mmWave) fragmented antenna with a single feed point is presented. The conductor region of the antenna aperture is approximately 0.5 mm by 2.0 mm or 0.07 λ x 0.25 λ at the shortest wavelength of operation. The antenna was fabricated on a 1.97 mm thick Rogers 5880LZ substrate using standard etching processes. Prior to fabrication, the antenna design was simulated across two different full-wave electromagnetic (EM) solvers, HFSS and GTRI's in-house finite-difference time-domain (FDTD) code; the two codes were in close agreement. The antenna prototype was characterized for reflection coefficient, realized gain, and principle plane patterns. These measurements closely agree with EM predictions.**

I. Introduction

THE last several decades have seen a steady increase in the number of mmWave antennas implemented for government and industry applications including imaging, precision tracking, high data rate communications, automotive collision avoidance, etc. This is due in large part to a desire for more compact antenna systems coupled with improvements in manufacturing processes allowing for smaller trace-and-space features on printed circuit board (PCB) technology. Also, ultrawideband (UWB) antennas help reduce the total number of antennas required on a given platform and thus improve the common radio frequency (RF) system metric known as CSWaP (cost, size, weight, and power).

In this paper a UWB mmWave antenna element with a single unbalanced feed point is presented with design, fabrication, and measurements. Unbalanced feeding schemes are uncommon for UWB planar antennas, either as a single element or in phased arrays. This is largely due to the susceptibility of imbalances in the current distribution across the aperture, which can cause undesirable effects such as asymmetric radiation patterns, high cross-polarization, and common-mode resonances. Instead, many UWB planar antennas such as bowties and multi-arm spirals are excited with a balanced, differential feed. This provides symmetry in the current distribution, assuming the aperture architecture is also symmetric on either side of the feed network. One style of unbalanced feeding for UWB planar arrays was introduced by introduced by Holland et. al in 2011 [1–5]. Whereas those designs were phased arrays, here a similar concept was applied to a single antenna element. These unbalanced feeding designs contain plated vias in the stack-up in order to help balance the current, mitigate common-mode resonances and generally to help match the antenna. It should be noted, however, that planar antenna designs containing vias are more conveniently implemented at higher frequencies, as the separation between the radiator and ground plane remains thin enough to construct the antenna with a single board as opposed to requiring multi-layer stack-ups. Given this shortcoming, GTRI recently designed an unbalanced wideband array (4.5:1) without vias entirely, but at the cost of efficiency [6].

This work is organized as follows. Section II will describe the antenna element in detail including physical dimensions, feeding scheme, and aperture type. Section III will explain the design procedure for this type of antenna. Section IV will present the results, both simulations and measurements of the final antenna design. Lastly, Section V will provide conclusions on this work and next steps for mmWave antennas of this type.

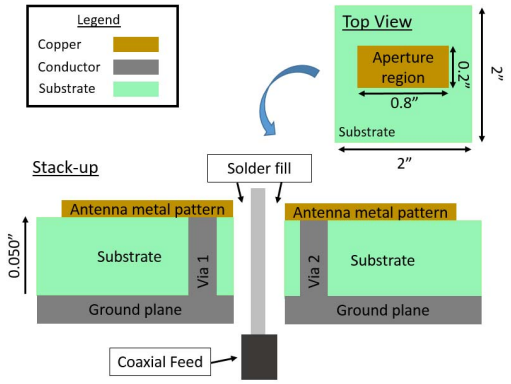

Figure 1. Illustrations of the antenna mechanicals: material stack-up (left) and top view (right) of the aperture board.

D.W. Landgren et al. are with the Georgia Institute of Technology, Georgia Tech Research Institute, Advanced Concepts Laboratory, Atlanta, GA, 30318 USA. *Corresponding author email: Kenneth.Allen@gtri.gatech.edu

978-1-5386-3200-0/17/$31.00 ©2017 IEEE

II. Description of the antenna

The antenna consists of a single PCB with the radiator on one layer and the ground plane on the other. The antenna element contains two plated vias and a single coaxial connector. The board material is Rogers 5880LZ with a thickness of 1.97 mm. The aperture region is approximately 0.2 mm by 5.0 mm 0.07 λ x 0.25 λ at the shortest wavelength (λ) of operation. A notional drawing of the stack-up and a top view of the antenna is shown in Fig. 1. As seen in Fig. 1, the board material extends beyond the aperture region; this helps prevent fringing fields from coupling to the backside of the ground plane.

The antenna aperture used in this work is known as a fragmented aperture [7–9]. This type of antenna consists of one or more layers of patterned metal, where the details of that patterning are determined by an optimization procedure, described in the section that follows. The fragmented aperture design from this work is shown in Fig. 2, where the color yellow represents conductor and white represents dielectric. As seen in the image, the element is symmetric about one axis and thus supports a single linear polarization.

The antenna targets operational frequencies from 18 GHz to 40 GHz with a specific gain profile based on the intended application. This gain profile includes a requirement to achieve 10 dBiL at broadside between 32 GHz and 38 GHz. The antenna is intended for receive-only application which allows for a relaxed goal for reflection coefficient; nevertheless, the goal was set to a nominal value of -10 dB.

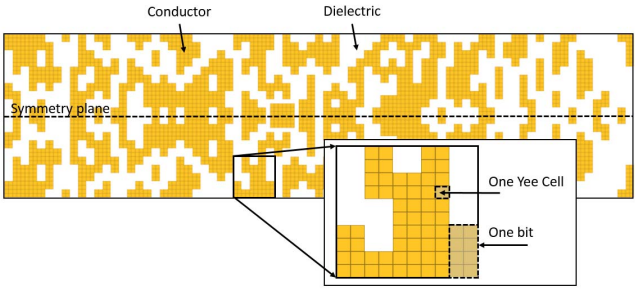

Figure 2. Example fragmented aperture geometry with a zoomed view indicating a single bits are formed by groups of FDTD Yee Cells of size 4 x 2.

III. Design Procedure

The antenna was designed with a fast in-house FDTD solver in concert with a multi-objective genetic algorithm, the latter provided by the open source Distributed Evolutionary Algorithms in Python (DEAP)

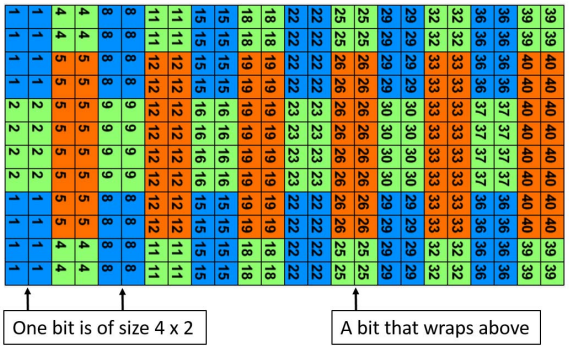

Figure 3. Basis function for the aperture design applied to a reduced footprint showing symmetry and two unique bit sizes formed by groups of FDTD Yee Cells of size 4 x 2.

suite. This technique has been leveraged for material characterization and generation of electromagnetic structures [10–13]. Both are critical to obtaining fragmented aperture designs efficiently as this type of antenna contains many degrees of freedom; for example, more than 100 bits (i.e. 2^{100} possibilities) is common. The inset in Fig. 2 shows that each bit for this design corresponds to groups of FDTD Yee Cells, in this case a 4 x 2 rectangle. The underlying geometry basis function is shown in Fig. 3 for a reduced footprint containing 40 total bits whereas the actual antenna contains 420 bits. The choice of basis function may include considerations for symmetry, feed location, and polarization. During the design process, each bit on the aperture can be turned on or off, indicating a placement of conductor or dielectric, respectively. This allows for a rich solution space corresponding to many different possible current distributions on the aperture.

The design process includes several key steps after the underlying geometry basis function has been chosen. Chief among these and prior to optimization of the antenna, is choosing a figure of merit; i.e., a method for objectively comparing each antenna candidate against another. Typically a single value is produced per objective called a "fitness" by comparing predicted performance to a predefined goal in some manner; e.g., realized gain vs. frequency.

$$\mathcal{F}_p(x_1, ..., x_n) = -\left(\frac{1}{N}\sum_{n=1}^{\infty}(x_i - g_i)^p\right)^{\frac{1}{p}} \qquad (1)$$

Equation 1 provides a simple calculation for generating a fitness value $\mathcal{F}_p$ by using the generalized mean. This calculation uses a given power level p from a set of performance data (x_1, x_2, ... , x_N) such as realized gain and a set of goal points (g_1, g_2, ... , g_N), each provided at the discrete frequencies from *1* to *N*.

The plots in Fig. 4 show two different fitness scores using this calculation for typical antenna specifications, gain and reflection, respectively. It is observed from the example in these graphs that the majority of the reflection RMS value in this case is produced by the contributions near the center and edges of the frequency band, where the antenna performs its worse relative to the goal. In order to prevent artificially boosting the fitness score at frequencies where the performance exceeds the goal, the score is often capped at 0.

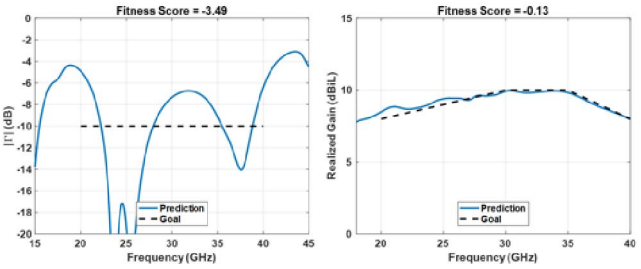

Figure 4. Example fitness scores of reflection coefficient (left) broadside gain (right).

After the previous steps are completed and a set of nominal codes are collated (wrappers, EM solver, FOM calculator, input/output scripts), the algorithm begins by sending an initial set of candidate antenna solutions to a high performance computing (HPC) cluster. These candidates can be random or a set of known candidates commonly referred to as a seed. From there, each candidate antenna is simulated and the fitness values are calculated. The best performing antennas are selected and bred (crossover) with the others and some randomness is added to the genes of the antenna as mutation. If the predicted performance ever reaches the goal (i.e., a fitness value near 0) or the fitness numbers are no longer appreciably improving, the program has converged.

After a result is found and prior to fabrication of the antenna, the converged design can be verified in an independent EM solver. In this case, the frequency-domain code HFSS was chosen because the conductors in FDTD are infinitesimal, and thus conductor losses were not accounted for, a potential concern at higher frequencies of operation where the fabricated thickness of the metal (i.e. roughly 2 μm) becomes more electrically significant. Fig. 5 shows a comparison of reflection coefficient and broadside gain performance for an earlier design under this effort; the two EM codes are in good agreement.

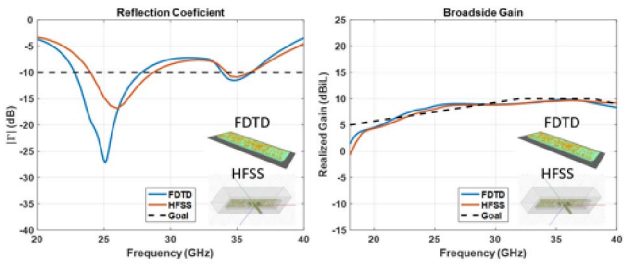

Figure 5. Independent simulations using an FDTD model and an HFSS model of a candidate antenna (left) for reflection coefficient (center) and realized gain at broadside (right).

IV. Results

To ensure measurement repeatability, the antenna required an additional set of parts to house the cable/connector assembly properly behind the ground plane of the antenna. The resulting fixture consists of a second board of standard FR4 material , positioned a set distance away using four plastic standoffs. The connector is bolted directly to this FR4 board with four screws and nuts. Fig. 6 shows a set of different images of the antenna and fixture parts including a close-up view of the aperture region near the feed / vias. It should be noted again that the antenna board was oversized to help prevent energy from coupling to the fixture housing.

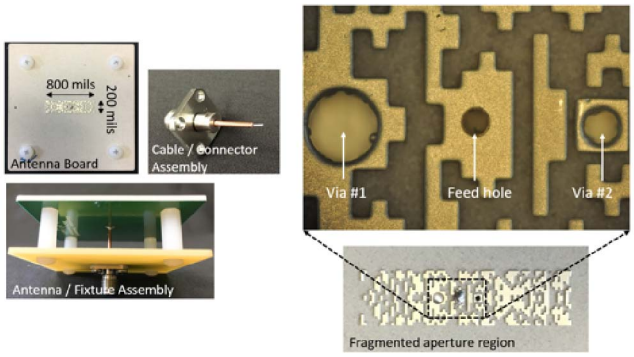

Figure 6. Images of antenna components including antenna board, fixture (with plastic standoffs and connector board), and custom cable (left). Images of the aperture are also shown including a close-up view of the fragmented aperture near the feed and vias (right).

After assembly, the antenna was measured in one of GTRI's antenna ranges using the two-antenna method for characterizing antenna gain. The range uses two standard horn antennas for calibration and the range is surrounded by absorbing material to help mitigate multipath and other potential measurement errors. Fig. 7 shows the reflection coefficient and broadside gain results versus predictions of the antenna. Fig. 8 shows E- and H-Plane measured and

predicted data for three frequencies: 32 GHz, 34 GHz, and 36 GHz. The measured results are in good agreement with the EM predictions.

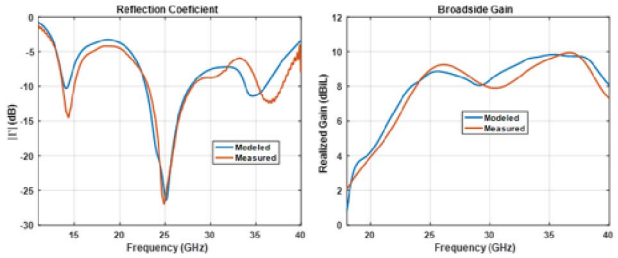

Figure 7. Model-measure agreement for reflection (left) and broadside gain (right).

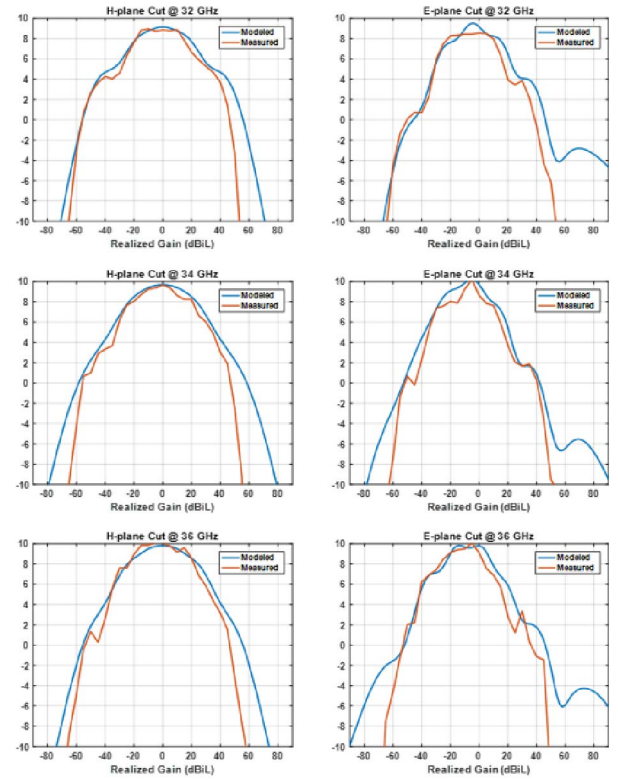

Figure 8. Model-measure agreement for principle plane cuts at 32 (top), 34 (center), and 36 GHz (bottom).

V. Conclusions

A UWB, mmWave antenna element was presented with simulated and measured results. The antenna contains a fragmented aperture which was designed using a fast in-house EM solver coupled with a genetic algorithm. The optimized final design was verified in the independent EM solver HFSS prior to fabrication. The antenna was assembled and measured in the range using the standard techniques. The measured results were found to be in good agreement with the predictions. Future work will include designing the antenna element without vias, adding a radome layer above the aperture, and designing for other polarizations.

References

[1] S. S. Holland and M. N. Vouvakis, "Design and fabrication of low-cost puma arrays," in *Antennas and Propagation (APSURSI), 2011 IEEE International Symposium on*. IEEE, 2011, pp. 1976–1979.

[2] S. S. Holland, D. H. Schaubert, and M. N. Vouvakis, "A 7–21 ghz dual-polarized planar ultrawideband modular antenna (puma) array," *IEEE Transactions on Antennas and Propagation*, vol. 60, no. 10, pp. 4589–4600, 2012.

[3] S. S. Holland and M. N. Vouvakis, "The planar ultrawideband modular antenna (puma) array," *IEEE Transactions on Antennas and Propagation*, vol. 60, no. 1, pp. 130–140, 2012.

[4] J. T. Logan, S. S. Holland, D. H. Schaubert, R. W. Kindt, and M. N. Vouvakis, "A review of planar ultrawideband modular antenna (puma) arrays," in *Electromagnetic Theory (EMTS), Proceedings of 2013 URSI International Symposium on*. IEEE, 2013, pp. 868–871.

[5] J. T. Logan and M. N. Vouvakis, "Planar ultrawideband modular antenna (puma) arrays scalable to mm-waves," in *Antennas and Propagation Society International Symposium (APSURSI), 2013 IEEE*. IEEE, 2013, pp. 624–625.

[6] D. W. Landgren, D. J. Dykes, and K. W. Allen, "An unbalanced feed design for wideband phased arrays," in *Proceedings of the International Telemeters Conference (ITC)*. ITC, 2017.

[7] J. Maloney, M. Kesler, P. Harms, T. Fountain, and G. Smith, "The fragmented aperture antenna: Fdtd analysis and measurement," in *Millennium Conference on Antennas and Propagation (AP 2000)*, 2000, p. 4.

[8] J. G. Maloney, M. P. Kesler, P. H. Harms, and G. S. Smith, "Fragmented aperture antennas and broadband antenna ground planes," Nov. 27 2001, uS Patent 6,323,809.

[9] J. G. Maloney, B. N. Baker, R. T. Lee, G. N. Kiesel, and J. J. Acree, "Wide scan, integrated printed circuit board, fragmented aperture array antennas," in *Antennas and Propagation (APSURSI), 2011 IEEE International Symposium on*. IEEE, 2011, pp. 1965–1968.

[10] D. S. Weile and E. Michielssen, "Genetic algorithm optimization applied to electromagnetics: A review," *IEEE Transactions on Antennas and Propagation*, vol. 45, no. 3, pp. 343–353, 1997.

[11] Y. Rahmat-Samii and E. Michielssen, "Electromagnetic optimization by genetic algorithms," *Microwave Journal*, vol. 42, no. 11, pp. 232–232, 1999.

[12] M. M. Scott, D. L. Faircloth, J. A. Bean, and K. W. Allen, "Permittivity and permeability determination for high index specimens using partially filled shorted rectangular waveguides," *Microwave and Optical Technology Letters*, vol. 58, no. 6, pp. 1298–1301, 2016.

[13] K. W. Allen, M. M. Scott, D. R. Reid, J. A. Bean, J. D. Ellis, A. P. Morris, and J. M. Marsh, "An x-band waveguide measurement technique for the accurate characterization of materials with low dielectric loss permittivity," *Review of Scientific Instruments*, vol. 87, no. 5, p. 054703, 2016.